Received: 23 July 2020 | Revised: 1 September 2020 | Accepted: 15 September 2020

DOI: 10.1002/maco.202011963

ARTICLE

Materials and Corrosion

Control of the diffusible hydrogen content in different steel phases through the targeted use of different welding consumables in underwater wet welding

Jan Klett[1] | Isabel B. F. Mattos[2] | Hans J. Maier[1] | Régis H. G. e Silva[2] | Thomas Hassel[1]

[1]Institut für Werkstoffkunde, Leibniz Universität Hannover, Garbsen, Germany

[2]Departamento de Engenharia Mecânica, LABSOLDA—Instituto de Soldagem e Mecatrônica, Centro Tecnológico, Universidade Federal de Santa Catarina, Campus Universitário, Trindade-Florianópolis, Santa Catarina, Brazil

Correspondence
Jan Klett, Leibniz Universität Hannover, Institut für Werkstoffkunde, An der Universität 2, 30823 Garbsen, Germany.
Email: klett@iw.uni-hannover.de

Funding information
Gottfried Wilhelm Leibniz Universität Hannover

Abstract

Due to the rising number of offshore structures all over the world, underwater wet welding has become increasingly relevant, mainly as a repair method. Welding in direct contact with water involves numerous challenges. A topic focused by many studies is the risk of hydrogen-induced cracking in wet weldments due to hardness values of up to 500 HV 0.2 in the heat-affected zone (HAZ) and high levels of diffusible hydrogen in the weld metal. The risk of cracking increases as the equivalent carbon content rises, because the potential to form martensitic structures within the HAZ rises too. Thus, high-strength steels are especially prone to hydrogen-induced cracking and are considered unsafe for underwater wet repair weldments.

KEYWORDS

arc voltage control, austenitic hydrogen traps, diffusible hydrogen, galvanic corrosion, hydrogen-induced cracking (HIC), SMAW, wet welding

1 | INTRODUCTION

The greatest challenges of the underwater wet welding process arise from the direct contact of the arc and the workpiece with the water. In the arc column, water is dissociated into hydrogen and oxygen due to temperatures of up to 5000°C. The oxygen reacts with alloying elements and partly removes them from the steel. Manganese and silicon, in particular, are affected by this oxidation. The effect is intensified with the increasing water depth.[1] In contrast, hydrogen can be absorbed by the melted weld pool and dissolved in the metal lattice. The diffusible atomic hydrogen is of particular importance. Due to the high thermal conductivity of water, the entire welding area cools down much faster in underwater wet welding, compared with a dry welding process.[2,3] Thus, hydrogen has significantly less time to leave the weld area by diffusion. The contents of diffusible hydrogen, which are measured after wet welding, range roughly from 26 to 100 ml/100-g weld metal. These values are significantly higher than those reported for dry onshore welding.[1,4–9] In addition, the rapid cooling leads to a quenching of the heat-affected zone (HAZ), and thus to the formation of martensite and/or bainite. Areas of high hardness are created. The impeded shrinkage causes additional stress in the workpiece. Together with the residual stresses resulting from the welding process, all risk factors that can lead to hydrogen-induced cold cracks are present.[10–12] This type of cracking is considered to be particularly

dangerous, because the damage is usually delayed, and sometimes even appears weeks after the actual welding.[11–13]

The risk of cold cracking is estimated by calculation of the carbon equivalent according to the formula[14]:

$$\mathrm{CEV}(\%) = \frac{\mathrm{Mn}(\%)}{6} + \frac{\mathrm{Cu}(\%) + \mathrm{Ni}(\%)}{15} + \frac{\mathrm{Cr}(\%) + \mathrm{Mo}(\%) + \mathrm{V}(\%)}{5}. \quad (1)$$

Steel with a CEV above 0.4% is not considered to be wet-weldable, because the hardness in the HAZ increases too much.[14] In the case of normalized rolled mild steels, the critical CEV value will usually be exceeded by steel with yield strengths above 350 MPa. Currently, high-strength steels are, therefore, considered as not suitable for underwater wet welding. The CEV is also included in the calculation of the heat treatment for dry welding tasks, but so far no heat treatment processes have been established under water. Current studies focusing on ultrasonic-assisted flux-cored arc welding show high potential.[15–17] However, the practical use of flux-cored arc welding is currently still limited by the commercially available equipment (e.g., underwater wire feeding). The only routinely employed way to weld high-strength steels is the application of the temper bead technique.[18–21] The principle here is the addition of a second weld seam with a little penetration depth on top of every necessary weld seam. This second, so-called "temper bead" is subsequently removed by grinding. It works like a postweld heat treatment for the first weld seam and provides a tempering effect in the HAZ.[20] However, the application of a weld seam with a little penetration depth and the subsequent grinding of the temper seam lead to a significantly increased effort for the diver, increased costs due to the additional electrodes, and longer diving times. Thus, the search for alternatives is the focus of many research works. Besides the strategy to use induction technology to provide a heat treatment,[22–24] and alteration of the stick electrode's cover,[7,25,26] the use of austenite-forming welding consumables was examined.[27–31] The solubility of hydrogen is significantly greater in the face-centered cubic austenitic phase than in the body-centered cubic lattice of the ferritic phase.[32] At the same time, the diffusion rate of hydrogen in austenitic iron is significantly reduced as compared with ferritic iron[32] (Figure 1). Hence, after underwater wet welding, the austenitic weld metal can trap more hydrogen. At room temperature, its diffusibility is strongly inhibited and diffusion from the austenitic lattice into the martensitic areas of the HAZ is very unlikely. Consequently, the risk of hydrogen-induced cracking can be reduced.[27]

Due to the different material properties of joints combining austenitic and ferritic steel, complex corrosion processes can occur. Specifically, galvanic corrosion, which is defined in ISO 8044,[33] is a crucial problem for these weld seams.[34] This form of corrosion occurs when two metals with different electrochemical potential are electrically connected, while they are immersed in an electrolyte. The electrolyte can be saline water, for example. In the case of an austenitic filler material used for welding ferritic/perlitic base materials, the corrosive attack will occur in the base metal or the HAZ, due to the less noble properties of these regions (compared with the austenitic weld metal). The expected weld corrosion is shown in Figure 2.

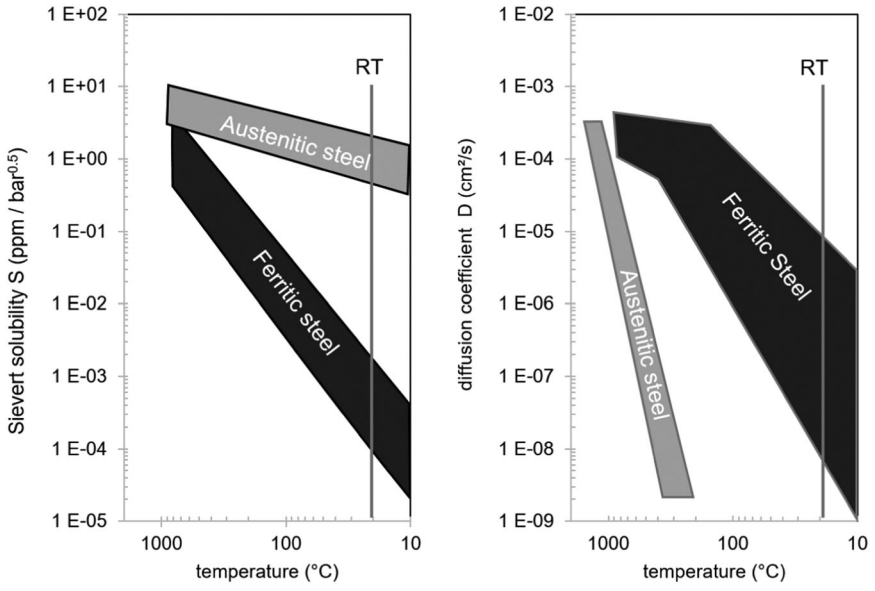

FIGURE 1 Solubility and diffusion coefficient of hydrogen in ferritic and austenitic steel depending on the temperature[32]

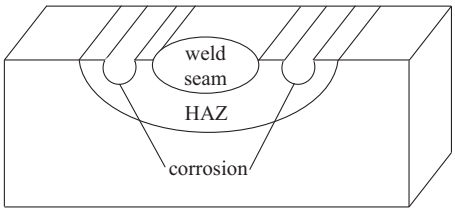

FIGURE 2 Galvanic corrosion on dissimilar welds (after Wahid et al.[34]). HAZ, heat-affected zone

To inhibit this type of corrosion, layers of ferritic weld metal can be used as covering layers above the austenitic root weld metal. This way, the areas of different electrochemical potentials are separated from the electrolyte, and the galvanic corrosion process should be stopped. The risk of hydrogen-induced cracking (HIC) for such covered austenitic weld roots has not been described yet.

The objective of this study was to investigate the content of diffusible hydrogen in ferritic, austenitic, and mixed austenitic–ferritic weldments. Ferritic weld seams were used to cover austenitic root welds to suppress galvanic corrosion. The influence of these covering layers of ferritic weld metal above the austenitic weld metal on the diffusible hydrogen content was of special interest.

For the present study, the weld metal of six different types of stick electrodes was analyzed regarding the diffusible hydrogen content. Suitable microstructures were first identified using calculations from the Schaeffler diagram. These calculations were then locally verified using Vickers hardness tests.

2 | METHODS

The automated welding machine used in the experiments had three separately controllable axes. Axes x and y are used for positioning and controlling the welding speed (v_s). Axis z controls the electrode's vertical position above the workpiece, and thus the arc-length during the welding process. For a constant arc-length, an arc voltage control system to adjust the electrode's feed rate was used. The experiments were performed in a water tank measuring $2.1 \times 3 \times 1$ m. The workpieces were fixed to a clamping device on the basis of the regulations of ISO 3690:2018.[35] All weldments were made at a water depth of 0.5 m. The electrodes were held at an angle of 90° to the workpiece in all tests. The welding polarity was DC- (as proposed by the stick electrodes' manufacturers). Two kinds of samples for diffusible hydrogen measurements were used. Both are composed of a run-on piece to ignite the arc, a run-off piece to finish the welding, and three sample pieces for diffusible hydrogen measurements placed in between the end pieces. Their dimensions are based on ISO 3690:2018 sample size C (width: 30 mm, length: 15 mm, and height: 10 mm),[35] and they are customized for multilayer fillet weldments (width: 30 mm, length: 15 mm, and height: 20 mm). The simultaneous usage of three samples is not recommended in the standard ISO 3690, but it was not found to interfere with the results.[36,37] Whereas the samples used for one and two weld seams strictly had the dimensions specified by the standard ISO 3690 size C, the samples used for triple-seam welds had a V-groove (45° inclination), as illustrated in Figure 3. The base material used for all samples was S235J2+N (CEV = 0.31%).

For the present study, six different grades of electrodes were used to compare the influences of different phases on the diffusible hydrogen content. Two of them were low-carbon ferritic, which are abbreviated as F1 and F2. Two stick electrodes created an iron-based chromium–nickel–austenitic weld metal, which are abbreviated as A1 and A2. One electrode had a stainless duplex steel wire (referenced to as D). The last electrode featured a nickel-base wire and is abbreviated as N. The welding parameters used are listed in Table 1. Using different parameters for each type of electrode improved the welding quality. This approach avoided low-quality weldments (e.g., excessive pores and inconsistent or uneven weld bead structure) in the data, which would have biased the analysis. The target arc voltage was optimized

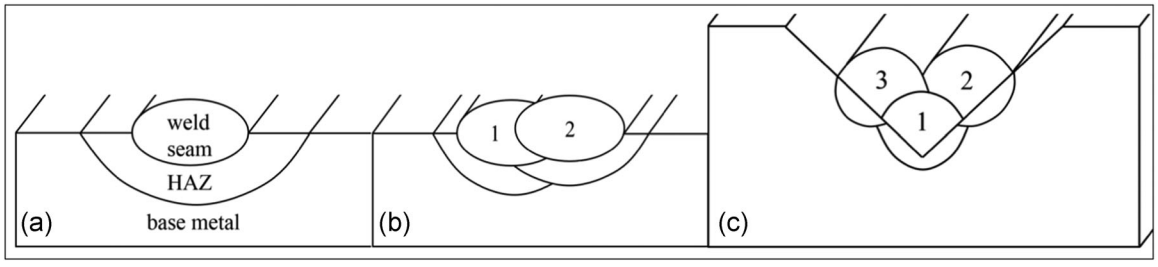

FIGURE 3 Sample dimensions: (a,b) $30 \times 15 \times 10$ mm (single and double seam); (c) $30 \times 15 \times 20$ mm (triple-seam) in a 45° V-groove

TABLE 1 Covered stick electrodes and parameters used

Electrodes' abbreviation	Developed for wet welding	Wire material	Commercially available	Welding current (A)	Target arc voltage (V)
F1	Yes	Ferritic steel	Yes	150	30
F2	Yes	Ferritic steel	Yes	150	30
D	Yes	Duplex steel	No[a]	150	27
A1	Yes	Austenitic Cr–Ni steel	No[a]	160	27
N	Yes	Nickel-base	Yes	130	26
A2	No[b]	Austenitic Cr–Ni steel	Yes	140	27

[a]Electrodes were provided by voestalpine Böhler for this project.

[b]Standard electrodes were coated with an alkyd resin sealing to be able to use them in a wet environment.

in preliminary tests to gain a stable arc during the whole welding process. The actual chemical compositions, as determined by optical emission spectrometry of the pure weld metal, are given in Table 2.

The welding speed v_s was held constant at 0.2 m/min for all experiments. The current and target voltage were adjusted separately for each individual electrode, as excessive defects in the weldments (e.g., pores) due to inappropriate process parameters might influence the results of the hydrogen analysis. Samples containing any kind of visible defects were sorted out and not measured. The double and triple weld seam samples were welded with a 60-s time gap between each seam. Within this time, the slag was removed entirely. The electrode combinations welded and analyzed are shown in Table 3.

After welding, the samples were stored in liquid nitrogen (lN_2), within 20 s after the arc extinguished, to prevent the hydrogen diffusion out of the sample. The cleaning and breaking of the samples were performed 30 min after the storage in lN_2, within 60 s. After 60 s, the samples were again put into lN_2 for at least 120 s, before the cleaning and breaking continued in accordance with ISO 3690:2018.[35] The clean samples were warmed to room temperature in water and washed in acetone. After cleaning with dry air, the samples were weighed (as before welding, a Mettler Toledo NewClassic MF scale was used; $d = 0.1$ mg) and analyzed in a Bruker G4 Phoenix diffusible hydrogen analyzer using the carrier gas hot extraction method. The samples were heated for 30 min at 400°C, to promote the diffusion of hydrogen out of the weld metal. After the analysis, the measured hydrogen volume was then referenced to the mass of the deposited weld metal (i.e., the difference of the mass of a sample before and after welding). This diffusible hydrogen content is referred to as H_D and is given in ml per 100-g weld metal. All times, sizes, temperatures, and methods are based on ISO 3690:2018.[35]

3 | RESULTS

The mean diffusible hydrogen contents in the differently welded samples are shown in Table 4 and in Figures 3–7. The values of the diffusible hydrogen content show a considerable variance (Table 4). Still, the difference in average hydrogen contents between different sample groups is substantial and large enough for interpretation.

TABLE 2 Optical emission spectrometry results of the pure weld metal (wt%)

Electrodes' abbreviation	C	Si	Mn	Cr	Ni	Mo
F1	0.06	0.31	0.39	0.03	0.03	0.61
F2	0.08	0.30	0.05	0.04	0.04	0.50
D	0.06	0.67	0.54	17.27	7.07	2.61
A1	0.06	0.58	0.63	16.08	25.70	3.05
A2	0.09	0.82	0.85	18.04	22.40	4.47
N	0.07	0.30	2.40	12.01	64.02	6.50

TABLE 3 Electrode combinations welded underwater at a water depth of 0.5 m (the individual welding parameters are given in Table 1)

First seam	Second seam	Third seam	Sample geometry (as shown in Figure 3)	Number of samples analyzed (*n*)
F1			a	15
F1	F1		b	9
F1	F1	F1	c	12
F2			a	12
F2	F2		b	14
F2	F2	F2	c	12
D			a	12
D	D		b	9
D	D	D	c	18
D	F1		b	12
D	F2		b	12
D	F1	F1	c	12
D	F2	F2	c	12
N			a	11
N	N		b	9
N	F1		b	15
N	F2		b	9
N	F1	F1	c	9
N	F2	F2	c	8
A1			a	6
A1	A1		b	6
A1	F1		b	6
A1	F1	F1	c	9
A2			a	9
A2	A2		b	9
A2	F1		b	9
A2	F2		b	9
A2	F1	F1	c	9
A2	F2	F2	c	9

3.1 | Weld samples produced with ferritic stick electrodes

The results of the samples welded solely with ferritic stick electrodes (F1 and F2) are illustrated in Figure 4.

TABLE 4 Diffusible hydrogen contents (H_D) and the corresponding standard deviations

Samples' abbreviation	H_D in ml/100-g weld metal (average)	Standard deviation
F1	61.02	6.92
F1–F1	52.94	6.85
F1–F1–F1	40.12	3.09
F2	62.65	6.28
F2–F2	52.46	8.85
F2–F2–F2	49.66	7.02
D	38.50	7.84
D–D	44.83	10.68
D–D–D	11.20	2.51
D–F1	38.97	7.46
D–F2	50.11	8.37
D–F1–F1	39.07	5.13
D–F2–F2	37.28	3.90
N	10.00	1.14
N–N	8.55	2.13
N–F1	29.35	7.24
N–F2	26.79	7.50
N–F1–F1	25.37	1.74
N–F2–F2	24.12	2.97
A1	7.89	1.69
A1–A1	8.14	1.30
A1–F1	53.53	5.11
A1–F1–F1	27.98	10.96
A2	5.05	0.69
A2–A2	4.24	1.01
A2–F1	25.17	3.45
A2–F2	26.01	3.45
A2–F1–F1	30.03	4.88
A2–F2–F2	27.49	4.94

A reduction of the mean diffusible hydrogen content by 13% (F1) and 16% (F2) is achieved by adding a second ferritic weld seam over the first one. The addition of a third seam reduces the mean diffusible hydrogen content by another 24% (F1) and 5% (F2). To determine if the means of two sets of data are significantly different from each other, the *t* test

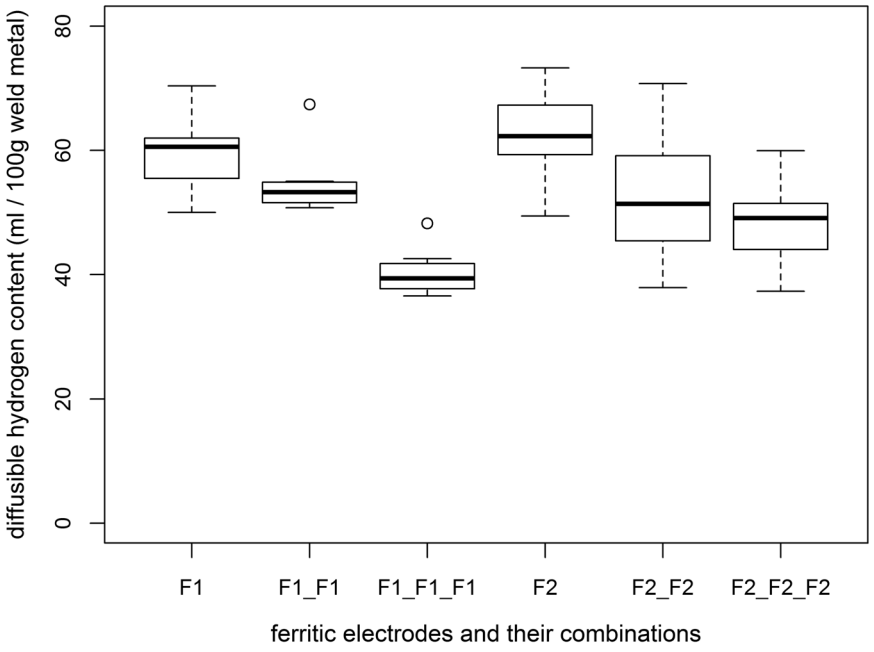

FIGURE 4 The boxplot of the diffusible hydrogen content in samples welded with ferritic root welds (see Table 1 for parameters); details of the boxplot: the horizontal line within the boxes represents the median, the boxes represent the interquartile range; the whiskers show the maximum or minimum of each distribution; outliners are marked with "o"

(α level .05) was used. Only the 5% reduction from F2−F2 to F2−F2−F2 is not significant.

3.2 | Weld samples produced with the duplex electrode

The results of all samples where the duplex stick electrode D was used as a root weld are shown in Figure 5. The mean hydrogen content does not significantly differ in most of these samples. The only significant differences appear in the samples composed of three duplex weld seams (D−D−D) and the samples featuring a duplex root weld covered with a single seam of the ferritic electrode F2 (D−F2).

3.3 | Weld samples produced with the austenitic stick electrodes

Figure 6 shows the results of the diffusible hydrogen measurement performed on samples welded with one or

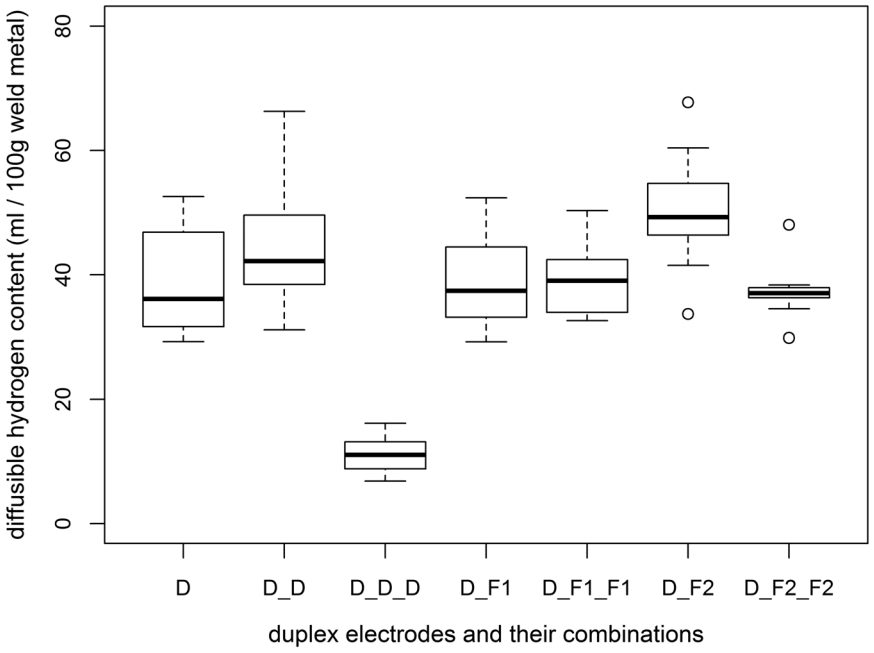

FIGURE 5 The boxplot of the diffusible hydrogen content in samples welded with duplex stick electrode root welds combined with duplex or ferritic covering (see Table 1 for parameters)

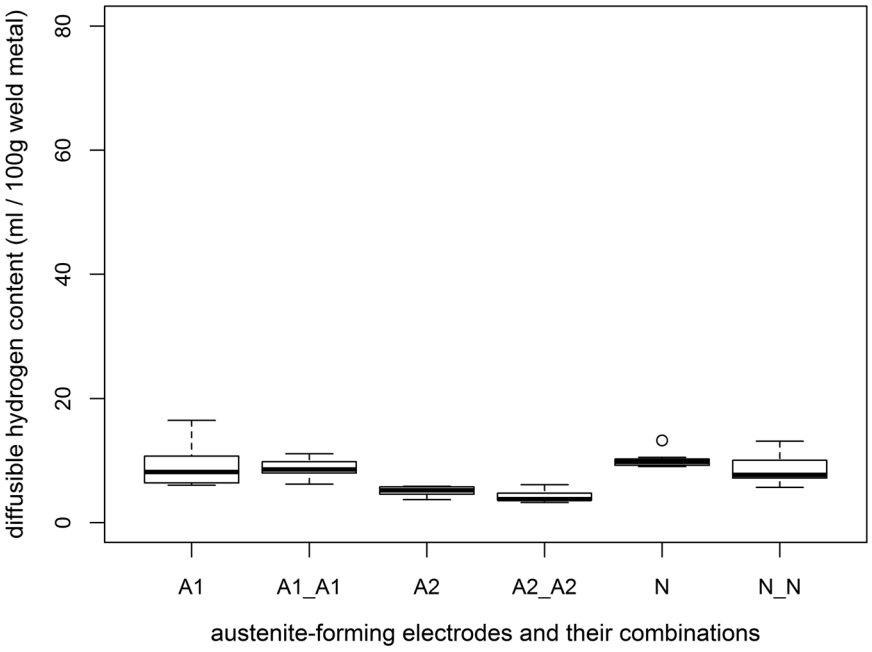

FIGURE 6 The boxplot of the diffusible hydrogen content in samples welded solely with austenitic stick electrodes (see Table 1 for parameters)

two austenitic weld seams, without ferritic additions to cover the root weld seams. This includes the root weldments performed with the Fe-based Cr–Ni–steel electrodes A1 and A2, as well as the weldments done with the Ni-based stick electrode N as a root weld, as these electrodes form austenitic weld metal too (when welded on mild steel). A comparison with the results of weldments without austenitic weld metal shows a reduction of the diffusible hydrogen content between 83% (comparing N with F1) and 92% (comparing A2–A2 with F1–F1). All 50 samples welded without ferritic stick electrodes showed diffusible hydrogen contents below 20 ml/100-g weld metal.

3.4 | Weld samples produced with ferritic electrodes as covering layers for root welds performed with the austenitic or nickel-base electrodes

Figures 7 and 8 show the austenitic root welds covered with one (Figure 7) or two (Figure 8) ferritic weld seams.

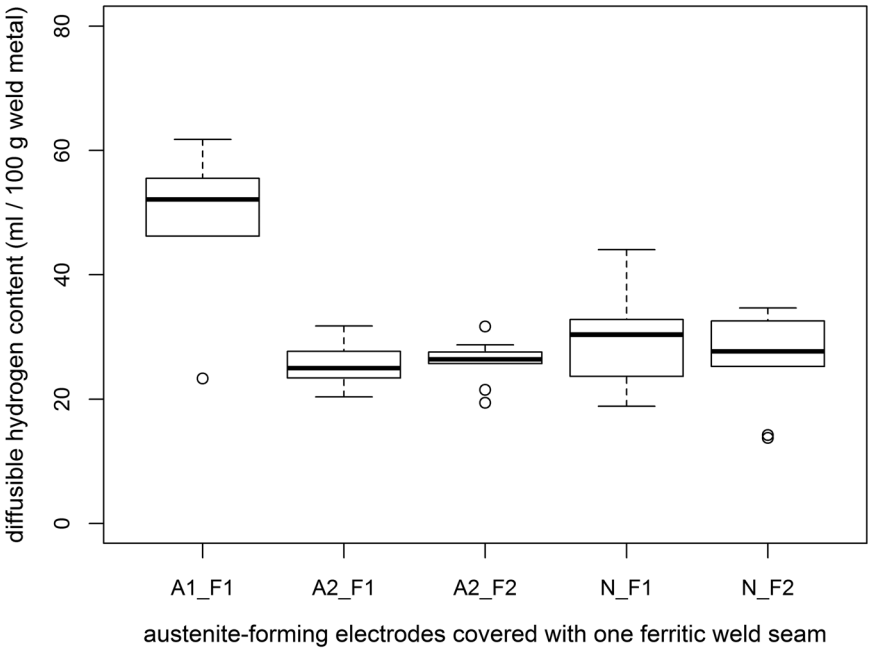

FIGURE 7 The boxplot of the diffusible hydrogen content in samples welded with one weld seam of the austenitic stick electrodes A1 and A2, or the Ni-based electrode N, covered with one ferritic weld seam (electrode F1 or F2) (see Table 1 for parameters)

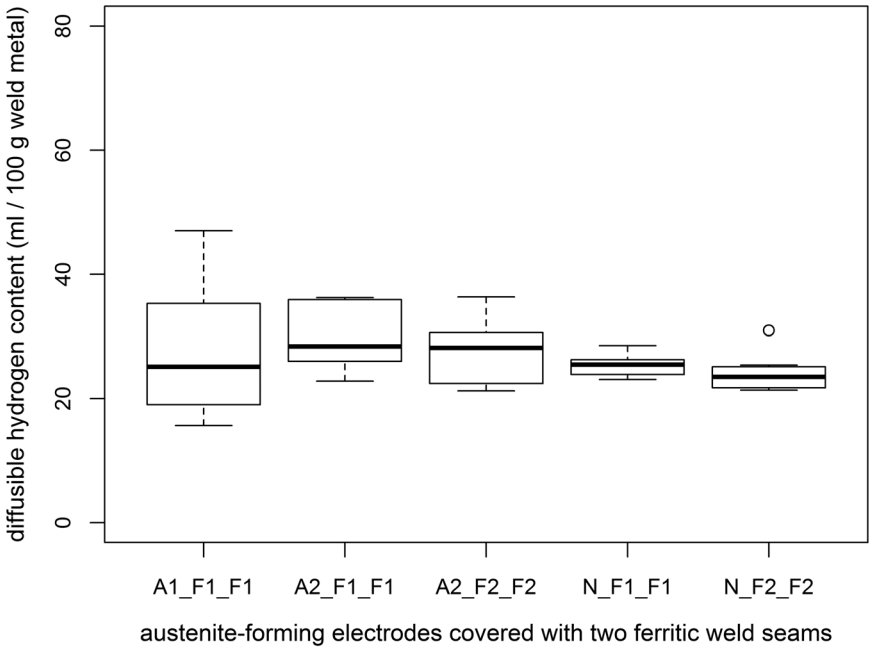

FIGURE 8 The boxplot of the diffusible hydrogen content in samples welded with one weld seam of the austenitic stick electrodes A1 and A2, or the Ni-based electrode N, covered with two ferritic weld seams (electrode F1 or F2) (see Table 1 for parameters)

The double weld seam samples combining the austenitic electrode A2 or the nickel-base electrode N with a ferritic electrode (N−F1, N−F2, A2−F1, A2−F2) show a significant reduction in the average diffusible hydrogen content, when compared with the respective samples in which both weld seams are made with ferritic electrodes (F1−F1 and F2−F2) (Figure 7 compared with Figure 4). The samples combining the nickel-base electrode with the ferritic electrodes F1 or F2 display a reduction of 46% and 42%, respectively. The samples combining the austenitic electrode A2 with the ferritic electrodes F1 or F2 show a reduction of 54% and 50%. Only the combination of A1−F1 does not show any reduction in comparison to F1−F1.

Similar results were found in the V-groove samples, where three seams were applied (Figure 8). The results obtained by the welding combination N−F1−F1 show a reduction of 37% in H_D as compared with F1−F1−F1. The difference of N−F2−F2 and F2−F2−F2 is 54%. A2−F1−F1 presents a reduction of 25% as compared with the results of F1−F1−F1, and 45% reduction is achieved by using A2−F2−F2 instead of F2−F2−F2. The difference in means between A1−F1−F1 and F1−F1−F1 amounts to 30%.

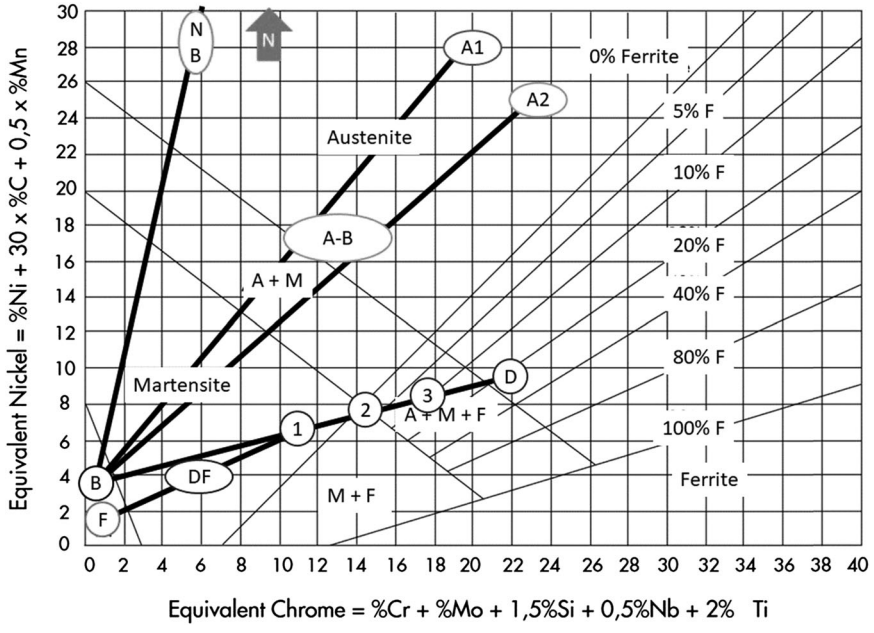

FIGURE 9 The Schaeffler diagram for the used materials: The base material is marked "B," the two Fe-based Cr−Ni−austenitic electrodes are marked "A1" and "A2," the Ni-based electrode is out of scale and marked by the arrow "N," and the duplex filler metal is marked "D"; "F" marks the ferritic steel stick electrodes F1 and F2

4 | DISCUSSION

Several different effects can be seen in these results. For the ferritic electrodes (Figure 4), the temper effect is visible. With the addition of more layers, more hydrogen from the lower layers can diffuse out of the material due to the reheating of the previous weld seam. This is similar to the effect of a short post-heating process, as described by Padhy et al.[38] The reduction of H_D is 13% from F1 to F1−F1 and 16% from F2 to F2−F2. The mean H_D value of F1 is 34% higher than the mean value of F1−F1−F1. For electrode F2, the difference between one and three layers is 21%. The temper effect should also affect the weldments performed with other electrodes as the root weld, but in these cases, the influence of the resulting microstructure is assumed to overshadow the effect of the reheating.

The results obtained for the duplex steel electrode D, the nickel-base electrode N, and the austenitic steel electrodes A1 and A2 are different and can be explained by analyzing the Schaeffler diagram (Figure 9). The microstructure of a welded combination can (under ideal circumstances) be found by drawing a line between the filler material and the base material, depending on the degree of dilution (e.g., a mixture of base material and filler material with a ratio of 1 to 1 would correspond to a point on the line in the middle of the two welded materials). The degree of dilution was estimated by measuring the areas in etched cross-section (2% nital etching performed on three samples of each type of hydrogen sample analyzed).

Point 1 marks the theoretical microstructure for the first layer of the duplex electrode welded on the ferritic base material. By welding a duplex electrode on ferritic base material, the weld becomes martensitic. This can be validated by looking at the hardness values (Figure 10). The hardness of the weld metal exceeds the hardness of the HAZ and reaches values above 500 HV 0.2. The sudden drop in hardness was investigated as well. These are cases where the Vickers indenter did hit cracks in the weld metal. These cracks could be found throughout the weld metal in samples welded with the duplex electrode.

Martensite is a tetragonally distorted form of ferrite that is supersaturated with carbon. The diffusible hydrogen content is lower here than in the microstructures solely welded with the ferritic stick electrodes F1 and F2. However, it shows higher diffusible hydrogen contents than the austenitic microstructures (e.g., A1 and A2; see Table 4). Applying the second weld seam of the duplex electrode (D−D) leads to Point 2 in Figure 9. There should be some ferritic and fewer austenitic parts in the microstructure now, but it remains mostly martensitic. When the third duplex weld seam is added (D−D−D),

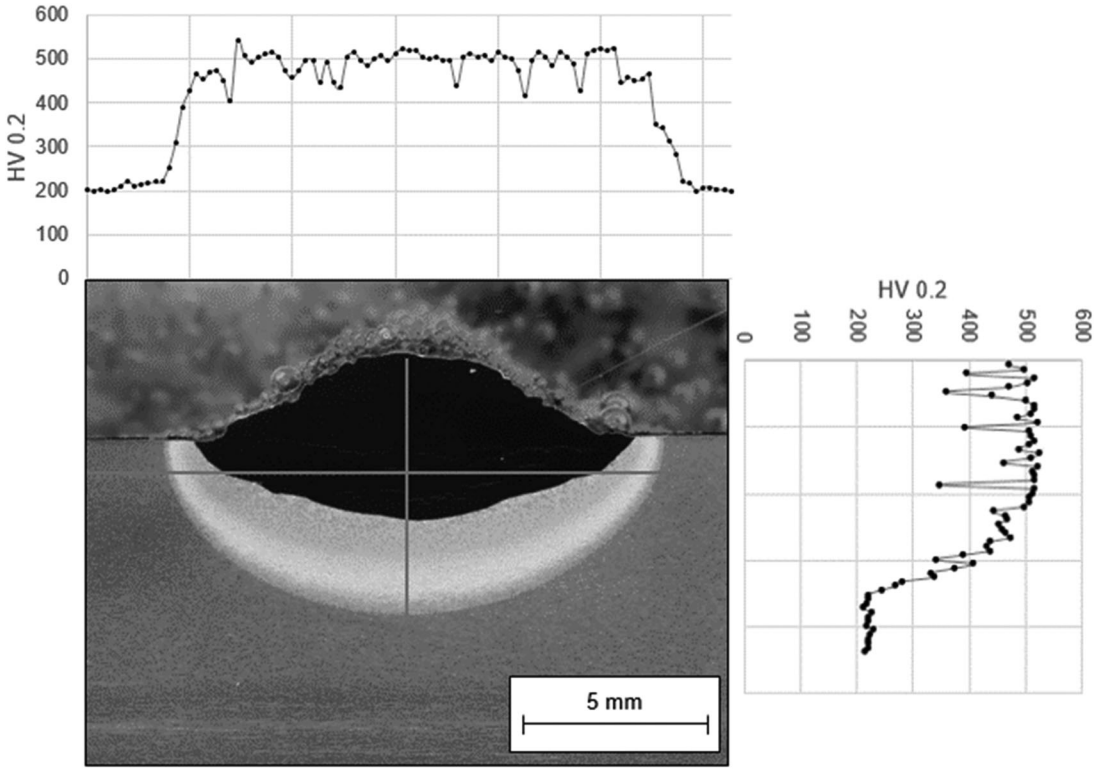

FIGURE 10 Hardness of the duplex root weld, measured in two directions (horizontal: top; vertical: right)

Point 3 in Figure 9 should be reached. Thus, the duplex electrode finally adds a noteworthy amount of austenite, while the lower layers are simultaneously tempered. The diffusible hydrogen content is drastically lowered (Figure 5).

When covering the duplex electrode with ferritic electrodes (D−F1, D−F2, D−F1−F1, and D−F2−F2), the whole weldment stays in the martensitic area (Area DF in Figure 9). The diffusible hydrogen remains (within the variance) the same for D, D−D, D−F1/D−F2, and D−F1−F1/D−F2−F2 combinations (see Figure 5). These consumable combinations form a mainly martensitic microstructure.

The point "A−B" in Figure 9 marks the root weld of the austenitic electrodes "A1" and "A2," welded on the ferritic base material "B." Point "N−B" marks the root weld of the nickel-base electrode "N," welded on the ferritic base material "B." In these cases, the root weld forms austenite, which is verified by the hardness measurements. Figure 11 shows the hardness measured in a weld seam cross-cut of the austenitic weld metal, welded with the Ni-based electrode. The hardness of the austenitic weld metal is less than the hardness of the ferritic/perlitic base metal. The addition of more layers of the same electrode will create more austenite (Figure 9).

The hydrogen values are accordingly low (Figure 6). These findings are in accord with the results obtained by Gooch[39] and Ozaki et al.[11]

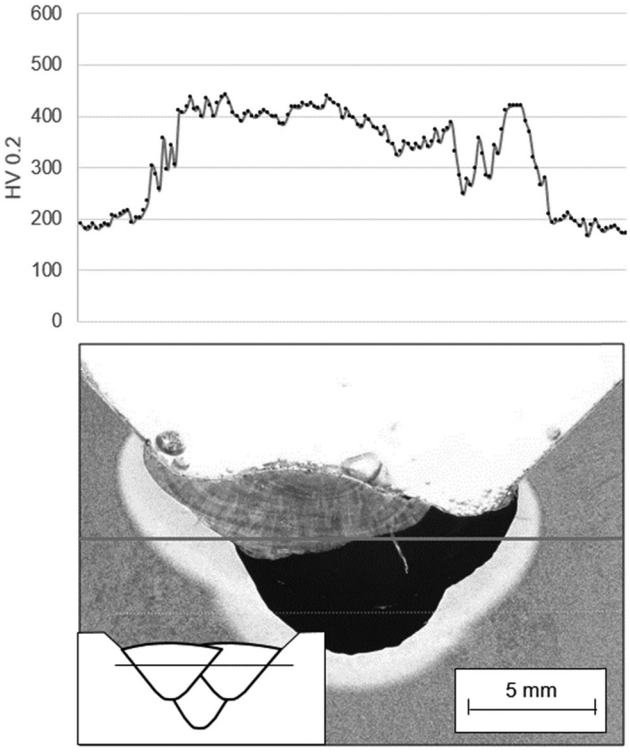

FIGURE 12 Hardness measured horizontally in the covering layer over an austenitic root weld, where the root was welded with the Ni-based austenitic electrode and covered with two ferritic weld seams; the second seam shows martensitic and tempered martensitic areas (tempered by the third seam), and the third seam is harder than the HAZ

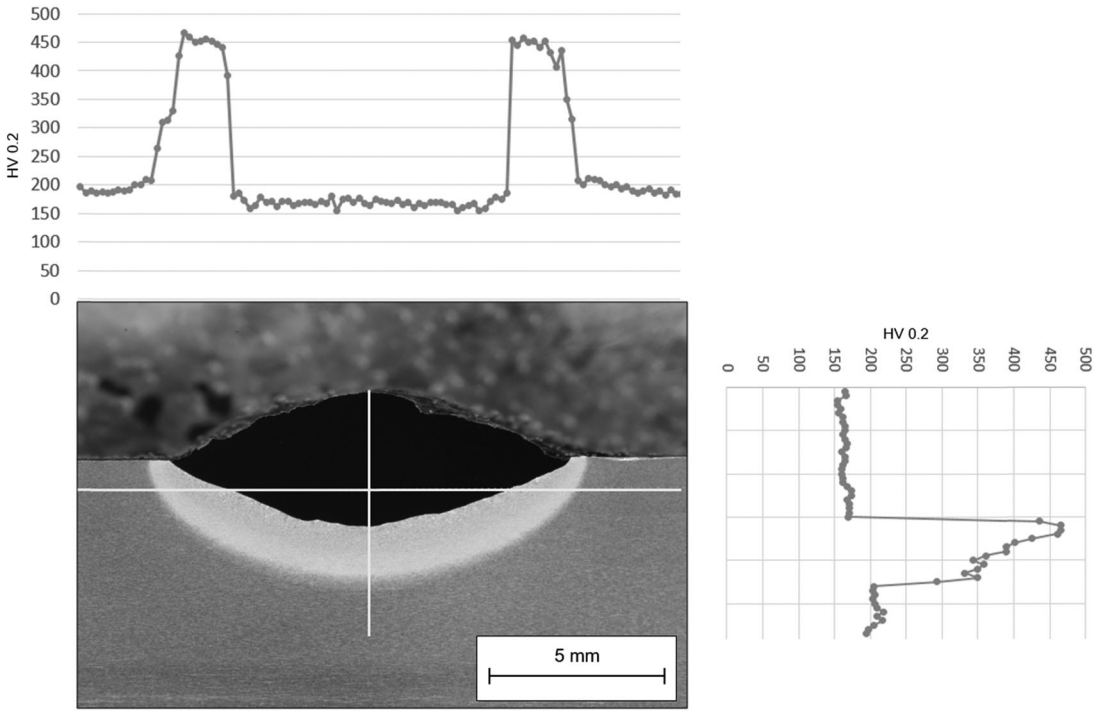

FIGURE 11 Hardness of the Ni-based austenitic root weld, measured in two directions (horizontal: top; vertical: right)

However, the addition of one or multiple ferritic layers will create a mostly martensitic structure in the diluted parts with only small austenitic shares (see Figure 9). Hardness measurements showed that some small areas of the root seam remained austenitic, whereas the other seams became martensitic with shares of tempered martensite in the second seam, when three seams were welded (Figure 12). This resulted in lower diffusible hydrogen values than in the austenite-free martensitic microstructure of D, D−D, D−F1, D−F2, D−F1−F1, and D−F2−F2 (Figure 5), but higher values than N and A1/A2 single- and double-layer welds (Figure 6). This tendency can be seen in all the hydrogen boxplots of the Ni-based and the Fe−Cr−Ni−austenite electrodes, covered with ferritic electrodes. The only exception is A1−F1 (Figure 7). These weldments and measurements were, thus, repeated, but no significant changes were found.

All samples besides A1−F1 (excluded due to the yet unexplained behavior) were grouped on the basis of the formed microstructure (the HAZs are not considered, as the volume of the diluted weld metal and molten base metal is much larger):

- F: Ferritic (F1, F2: without temper effect)
- M: Mainly martensitic (M = D, D−D, D−F1, D−F2, D−F1−F1, D−F2−F2)
- MA: Martensitic−austenitic (with tempered martensitic shares) (MA = A1−F1−F1, N−F1, N−F2, N−F1−F1, N−F2−F2, A2−F1, A2−F2, A2−F1−F1, A2−F2−F2)
- A: Mainly austenitic (A = A1, A1−A1, A2, A2−A2, N, N−N, D−D−D)

Within the groups M and MA, no significant difference between the individual results were found. For group A, the values involving A2 are significantly lower than the others, but are included, as the value range is quite low, compared with the variance. Group F, containing the nontempered ferritic microstructures of F1 and F2 single-layer welds, is also homogenous. A boxplot comparing these groups is shown in Figure 13. These groups show significant differences (test: analysis of variance: $p < .05$).

This study was carried out with the objective of reducing the diffusible hydrogen content in wet weldments by adding austenitic weld metal. The austenite should work as a hydrogen trap, and thus should decrease the risk of hydrogen-induced cold cracking.

The results show that there is a significant difference in diffusible hydrogen contents for samples welded with different grades of electrodes. The resulting microstructures are divided in four groups: Mainly ferritic, mainly martensitic, martensitic−austenitic, and mainly austenitic. These four groups show significantly different diffusible hydrogen contents, regardless of the electrode combinations that were used to form the microstructures.

The difference in diffusible hydrogen is achieved by trapping hydrogen, which is not diffusible at room temperature. It can be concluded that martensite can trap more hydrogen than ferrite and austenite can trap more hydrogen than martensite. Martensite with austenitic shares traps more hydrogen than pure martensite, but less than austenite.

All samples welded in this study, which were not tempered by a second or third weld seam, showed high

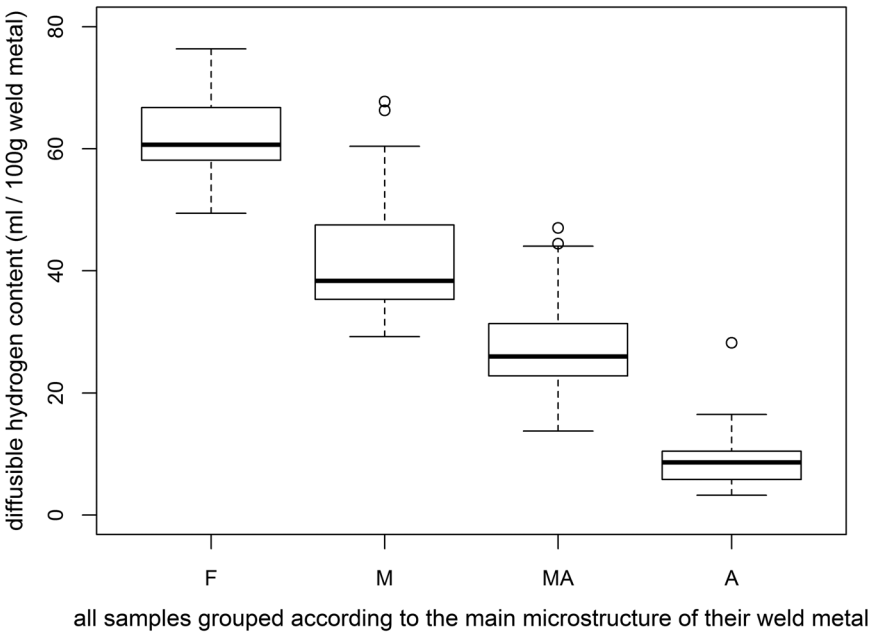

FIGURE 13 The boxplot of diffusible hydrogen content for the different microstructures formed in the welding process. A, mainly austenitic; F, ferritic; M, mainly martensitic; MA, martensitic−austenitic

hardness in the HAZ. The reduction of the diffusible hydrogen content can still reduce the HIC risk, as shown in a previous study that used a novel test.[27] Thus, changing the microstructure of a weldment can reduce the HIC risk by reducing the diffusible hydrogen content. However, not all variants are applicable for underwater wet welding. The formation of extended amounts of martensite will lead to very hard and brittle weldments; thus, the combinations welded with both ferritic and austenitic electrodes are not useful for actual applications. The same applies for weldments done with the duplex electrode. Using austenitic electrodes without a ferritic covering layer is the only reasonable method to obtain low diffusible hydrogen contents. There are some limiting factors to be considered: The different solidification points of the base metal and the filler material favor solidification cracks and cavities. Further research is necessary to explore these factors more deeply. Additionally, the water depth might be limiting to the application of some electrodes. Nickel electrodes tend to generate more pores in wet weldments than ferritic electrodes.[39,40] Another challenge lies in the materials used: The ferritic/perlitic base material and the austenitic weldment will form a local cell with the increased risk of galvanic corrosion. Whereas the open circuit potential difference between the weld metal welded with ferritic stick electrodes and the ferritic/perlitic base material was below 100 mV, the difference between the austenitic weld metal of the Ni-based stick electrode and the ferritic/perlitic base material amounted to 436 mV, which appear critical with respect to galvanic corrosion. Forms of protection, other than ferritic covering layers, are needed, and work is underway to address this issue.

5 | CONCLUSIONS

In the present study, austenitic weld deposits were employed to reduce the amount of diffusible hydrogen present in underwater wet weldments. They were either covered with additional austenitic layers or with ferritic layers. The main results can be summarized as follows:

1. Whereas ferritic covering layers can seal the austenitic root weld and prevent galvanic corrosion, the dilution of ferritic and austenitic weld metal leads to brittle martensitic weldments.
2. Austenitic weld metal can trap more hydrogen than ferritic or martensitic weld metal. This leads to a reduction of diffusible hydrogen content of up to 91.72%, comparing a ferritic weld seam with an austenitic weld seam.
3. Martensitic weld metal can trap more hydrogen than ferritic weld metal, but less than austenitic weld metal. The diffusible hydrogen content is lower than that in ferritic weld metal but higher than that in the austenitic weld metal. It is reduced when more austenite is added.
4. If more than one weld seam is applied, the tempering effect lowers the diffusible hydrogen content. A reduction of 34.25% was achieved by covering a ferritic weld seam with two additional ferritic weld seams of the same grade.
5. The diffusible hydrogen content can get below 5 ml/100-g weld metal when two layers of austenitic welding consumables are applied.

ACKNOWLEDGMENTS

The authors thank Kjellberg Finsterwalde Elektroden und Zusatzwerkstoffe GmbH and voestalpine Böhler Welding UTP Maintenance GmbH for supporting this study by providing welding consumables. This study was a part of the DVS research project IGF 19.211N funded by the AiF as a part of the program to support "Industrial Community Research and Development" (IGF) funded by the Federal Ministry for Economic Affairs and Energy on the basis of a decision of the German Bundestag. A part of this study was conducted during a scholarship program supported by the International Cooperation Program CAPES at the University of Santa Catarina, financed by CAPES, Brazilian Federal Agency for Support and Evaluation of Graduate Education within the Ministry of Education of Brazil. Open access funding enabled and organized by Projekt DEAL.

CONFLICT OF INTERESTS

The authors declare that there are no conflict of interests.

DATA AVAILABILITY STATEMENT

The data that support the findings of this study are available from the corresponding author upon request.

ORCID

Jan Klett http://orcid.org/0000-0002-3139-5506

REFERENCES

[1] S. M. Kussike, *PhD Thesis*, Leibniz Universität (Hannover, Germany) **2015**.
[2] K. A. Yushchenko, Y. Y. Gretskii, S. Y. Maksimov, presented at Underwater Wet Weld. Cutting: Int. Sem. Workshop TWI North, Middlesbrough, UK, April **1997**, 6–30.
[3] J. Łabanowski, D. Fydrych, G. Rogalski, *Adv. Mater. Sci.* **2008**, *8*, 11.
[4] A. Świerczyńska, D., Fydrych , G., Rogalski , *Int. J. Hydrogen Energy* **2017**, *42*, 24532.
[5] V. Hecht-Linowitzki, J. Klett, T. Hassel, *Schweißen und Schneiden* **2018**, *70*, 720.

[6] X. Kong, C. Li, Y. Zou, J. Zhang, Y. Hu, J. Wang, presented at MATEC Web Conf. 39 **2016**, 03004-p1–03004-p5. https://doi.org/10.1051/matecconf/20163903004
[7] J. Tomków, D. Fydrych, K. Wilk, *Materials* **2020**, *13*, 2947.
[8] W. C. D. da Silva, L. F. Ribeiro, A. Q. Bracarense, presented at ASME 2012 31st Int. Conf. Ocean, Offshore Arctic Eng. OMAE2012-83002, No. 44939 **2012**, pp. 1–8.
[9] D. Fydrych, A. Świerczyńska, G. Rogalski, *Metall. Ital.* **2015**, *11/12*, 47.
[10] J. C. Lippold, *Welding Metallurgy and Weldability*, John Wiley & Sons, Hoboken, NJ **2014**.
[11] H. Ozaki, J. Naiman, K. Masubuchi, *Weld. J.* **1977**, *8*, 231.
[12] J. Tomków, J. Łabanowski, D. Fydrych, G. Rogalski, *Polish Marit. Res.* **2018**, *25*(*No. 3*), 131.
[13] D. Fydrych, G. Rogalski, J. Labanowski, *Inst. Weld. Bull.* **2014**, *58*, 187.
[14] Deutscher Verband für Schweisstechnik e.V., DVS Merkblatt 1818 **2017**.
[15] H. Chen, N. Guo, K. Xu, C. Xu, L. Zhou, G. Wang, *Mater. Des.* **2020**, *188*, 108482.
[16] Q. J. Sun, W. Q. Cheng, Y. B. Liu, J. F. Wang, C. W. Cai, J. C. Feng, *Mater. Des.* **2016**, *103*, 63.
[17] H. Chen, N. Guo, C. Liu, X. Zhang, C. Xu, G. Wang, *Int. J. Hydrogen Energy* **2020**, *45*, 10219.
[18] J. Tomków, D. Fydrych, G. Rogalski, *Materials* **2019**, *12*, 3372.
[19] J. Tomków, G. Rogalski, D. Fydrych, J. Łabanowski, *J. Mater. Process. Technol.* **2018**, *262*, 372.
[20] P. Szelagowski, *Underwater welding technology: Fundamentals, Research and Applications*, DVS Media, Düsseldorf, Germany **2015**.
[21] J. Tomków, D. Fydrych, G. Rogalski, J. Łabanowski, *Adv. Mater. Sci.* **2018**, *18*, 5.
[22] H. T. Zhang, X. Y. Dai, J. C. Feng, L. L. Hu, *Weld. J.* **2015**, *94*, 8s.
[23] O. Brätz, K.-M. Henkel, J. Klett, T. Hassel, presented at Kolloquium Induktionserwärmung in der schweißtechnischen Fertigung, Halle (Saale), Germany, October **2018**, pp. 29–35.
[24] U. Reisgen, S. Olschok, K. Lenz, *Schweißen und Schneiden* **2018**, *70*, 396.
[25] V. R. Santos, M. J. Monteiro, F. C. Rizzo, A. Q. Bracarense, E. C. P. Pessoa, R. R. Marinho, L. A. Vieira, *Weld. J.* **2012**, *12*, 319s.
[26] P. H. R. Menezes, E. C. P. Pessoa, A. O. Bracarense, *J. Mater. Process. Technol.* **2019**, *266*, 63.
[27] J. Klett, T. Hassel, *Weld. Cutting* **2020**, *19*, 54.
[28] M. Rowe, S. Liu, *Sci. Technol. Weld. Joining* **2001**, *6*, 387.
[29] H. Li, D. Liu, Y. Song, Y. Yan, N. Guo, J. Feng, *J. Mater. Process. Technol.* **2017**, *249*(*Suppl C*), 149.
[30] S. J. Findlan, G. J. Frederick, International symposium of Materials ageing and component life extension, 10-13 October, Milan, Italy. In: Bicego, V., Editor. Engineering materials advisory services (EMAS); Vol. 1, 1995, p. 979.
[31] N. Guo, Z. Yang, M. Wang, X. Yuan, J. Feng, *Strength Mater.* **2015**, *47*, 12.
[32] H. Pircher, R. Großterlinden, *Mater. Corros.* **1987**, *38*, 57.
[33] DIN—Deutsches Institut für Normung e. V., DIN EN ISO 8044 **2015**.
[34] A. Wahid, D. L. Olson, D. K. Matlock, *ASM Handbook* **1993**, *6*, 1065.
[35] International Organization for Standardization, ISO 3690 **2018**.
[36] J. Klett, T. Wolf, H. J. Maier, T. Hassel, *Materials* **2020**, *13*, 3750.
[37] J. Klett, V. Hecht-Linowitzki, O. Grünzel, E. Schmidt, H. J. Maier, T. Hassel, *SN Appl. Sci.* **2020**, *2*, 1269.
[38] G. K. Padhy, V. Ramasubbu, N. Murugesan, C. Remash, S. K. Albert, *Sci. Technol. Weld. Joining* **2012**, *17*, 408.
[39] T. G. Gooch, *Met. Constr.* **1983**, *3*, 164.
[40] P. Szelagowski, H. Stühff, H. G. Schafstall, J. Blight, I. Pachniuk, *Weld. Int.* **1993**, *7*, 345.

How to cite this article: Klett J, Mattos IBF, Maier HJ, e Silva RHG, Hassel T. Control of the diffusible hydrogen content in different steel phases through the targeted use of different welding consumables in underwater wet welding. *Materials and Corrosion*. 2021;72:504–516. https://doi.org/10.1002/maco.202011963